

Figure 2 Schematics of the LM-based meander coil with distributed capacitors: (a) Configuration of the WPT clothing, (b) Conventional jointing method using adhesive force, (c) Proposed jointing method using friction force.

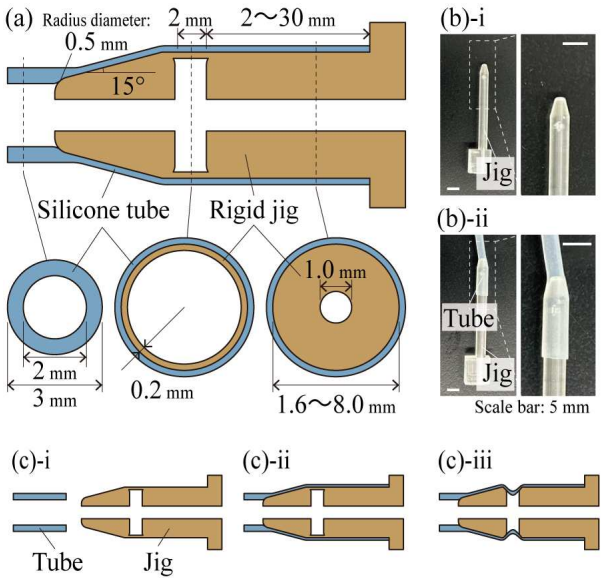


Figure 3 Experimental samples for stretching and bending tests of friction-based jointing: (a) Cross sections, (b) Photographs, (c) Fabrication procedures.

inner diameter of the jig is 1.0 mm, and the length of the jig (L_{jig}) is from 2 to 30 mm. The cone apex angle is 30° , and the cone tip has a radius of curvature of 0.5 mm. The separation area is 0.2 mm thick. The tube is pulled parallel and perpendicular to the jig in the tensile and bending tests, respectively, to investigate the frictional force and breakage of the jig and tube.

Figure 4 shows the cross sections and photographs of the frictional jointing of a capacitor and LM-based coil. A

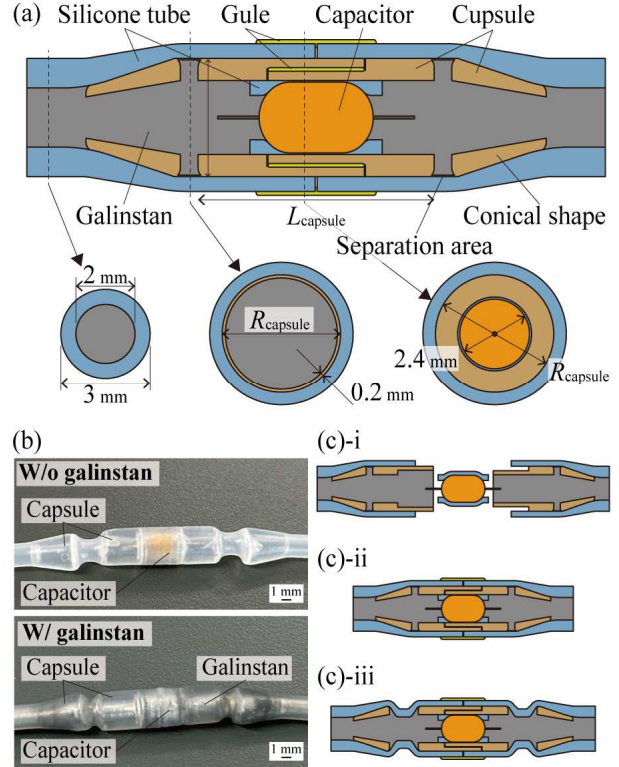


Figure 4 Friction-based jointing between capacitors and rubber tube filled with galinstan: (a) Cross sections, (b) Photographs, (c) Fabrication procedures.

lead capacitor (AxiMax 400 Comm C0G, KEMET, USA) covered with a rigid capsule is jointed with rubber tubes filled with galinstan (Sichuan HPM, China), as shown in Figures 4(a) and (b). Galinstan has high conductivity (10^6 S/m) and stretchability ($>400\%$)^{[6],[7]}. A capacitor with a thin rubber tube was covered with a capsule and inserted into the rubber tubes. The ends of the tubes are sealed with adhesive glue to prevent leakage. The outer diameter ($R_{capsule}$) and length ($L_{capsule}$) of the capsule are 4.8 and 36 mm, respectively, based on the measurement results. Figure 4(c) shows fabrication procedures; tubes filled with galinstan and the capacitor covered with the capsule are assembled, and the tips of the capsules are separated.

RESULTS AND DISCUSSION

Figure 5 shows the measurement results of the stretch tolerance. As φ_{jig} and L_{jig} increased in Figures 5(a) and (b), the tube slipped off from the jig and the breakage force (F_{break}) increased. As φ_{jig} and L_{jig} increased further, the tube ruptured and F_{break} became constant. These results indicate that the frictional force increased and the stretch tolerance improved as φ_{jig} and L_{jig} increased. When sweeping φ_{jig} and L_{jig} , F_{break} increased and became constant as φ_{jig} and L_{jig} increased. The area surrounded by the red dotted line in Figure 5(c) shows the values of φ_{jig} and L_{jig} , where F_{break} was constant. These results indicate that the highest stretch tolerance can be obtained by increasing φ_{jig} and L_{jig} until the stretch tolerance of the tube is brought out.

Figure 6 shows the measurement results of the bending tolerance. For small φ_{jig} and L_{jig} , the tube slipped off from

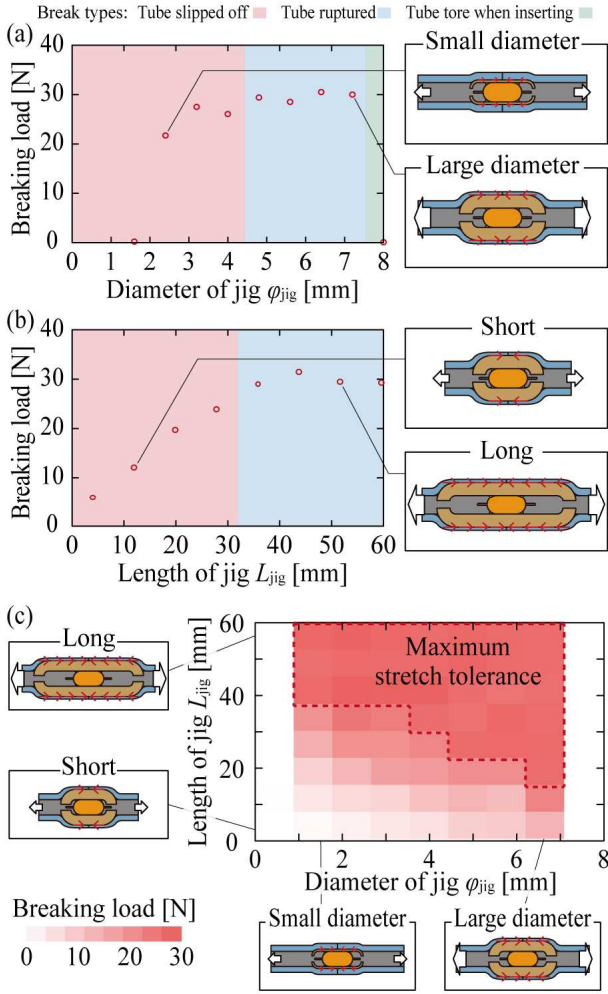


Figure 5 Experimental results of stretch tolerance: (a) Relationship between ϕ_{jig} and F_{break} breaking load ($L_{jig}=18$ mm, $N=3$), (b) Relationship between L_{jig} and F_{break} ($\phi_{jig}=4.8$ mm, $N=3$), (c) Mapping of F_{break} for ϕ_{jig} and L_{jig} ($N=3$).

the jig. As ϕ_{jig} increased in Figure 6(a), the jig broke and F_{break} increased. As ϕ_{jig} increased further, the tube ruptured and F_{break} decreased. As L_{jig} increased in Figure 6(a), the tube ruptured and F_{break} increased. As L_{jig} increased further, the jig broke and F_{break} decreased. These results indicate that the frictional force increased and the bending tolerance improved as ϕ_{jig} and L_{jig} increased. Within the range where the tube did not slip off, we found a trade-off relationship: the suppression of the breakage of the jig and the promotion of the difference in the bending stiffness between the jig and tube by using a thick and short jig. When sweeping ϕ_{jig} and L_{jig} in Figure 6(c), F_{break} increased and then decreased as ϕ_{jig} and L_{jig} increased, respectively. This trade-off relationship can be overcome and high bending tolerance can be achieved by increasing the toughness and flexibility of the capsule.

Figure 7 compares the stretch and bending tolerances of the jointing methods. Figure 7(a) shows the product of the stretch and bending tolerances normalized by their maximum values. The maximum stretch and bending tolerances were 31.8 and 25.9 N when ϕ_{jig} and L_{jig} were 4.8 and 18 mm, respectively. For comparison, stretch and

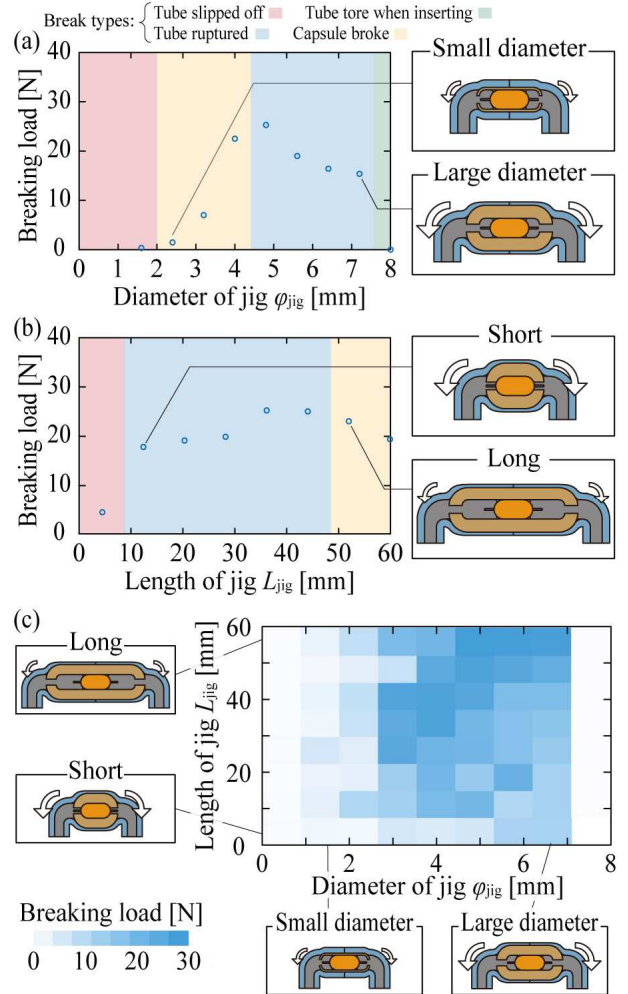


Figure 6 Experimental results of bending tolerance: (a) Relationship between ϕ_{jig} and F_{break} ($L_{jig}=18$ mm, $N=3$); (b) Relationship between L_{jig} and F_{break} ($\phi_{jig}=4.8$ mm, $N=3$), (c) Mapping of F_{break} for ϕ_{jig} and L_{jig} ($N=3$).

bending tolerances were measured for conventional adhesive glues: Aron Alpha Extra Jelly (TOAGOSEI, Japan), 1530C (ThreeBond, Japan), Super X (Cemedine, Japan), and Ultra-Versatile SU (KONISHI, Japan). Their average stretch and bending tolerances were 10.3 and 7.5 N, respectively as shown in Figures 7(b) and (c). The frictional jointing method achieved 3.1 times higher stretch tolerance and 3.5 times higher bending tolerance than the adhesive jointing method.

Figure 8 shows photographs of the WPT clothing by the friction jointing method. Figure 8(a) shows the Prototype of the WPT cardigans, sleeves, and trousers. The LM-based TX coil for the cardigan has eight capacitors of 270 pF attached at 90 mm intervals. The TX coil for the sleeve has six capacitors of 470 pF attached at 50 mm intervals. The TX coil for the trousers has 14 capacitors of 390 pF attached at 90 mm intervals. Their resonant frequency is adjusted to 6.78 MHz, the same as the AC source. The conductivity of the LM coil is 10^{-1} Ω /m and its weight is 27.8 g/m. The length and width of the RX coil are 20 mm and its resonant frequency is adjusted to 6.78 MHz. The inductance, resistor, and Q-factor of the RX coil are 3.3 μ H, 2.3 Ω , and 61, respectively. Figure 8(b) demonstrates WPT for five devices with multiple LEDs

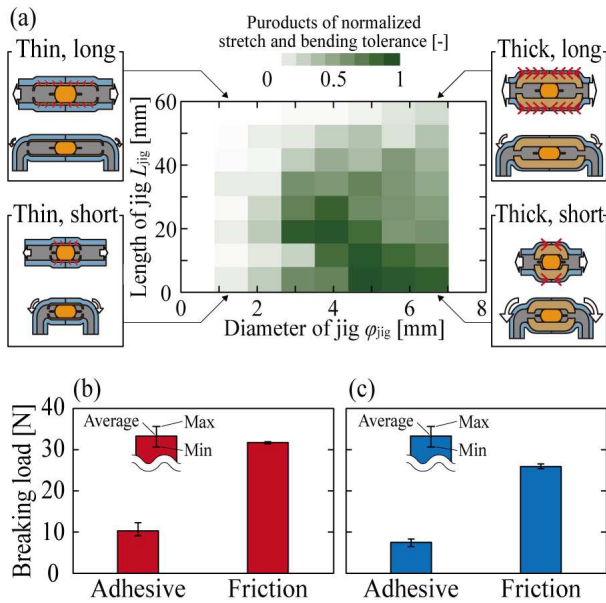


Figure 7 Comparison of stretch and bending tolerances for jointing methods: (a) Stretch and bending tolerances for the friction jointing method, (b) Stretch and (c) Bending tolerances for jointing methods ($N=3$).

placed on the cardigan, which requires Watt-class power supply. This result shows that watt-class WPT can be achieved for high-power wearable devices using our WPT clothing. Figure 8(c) shows photographs of the bending test. The sleeve was attached to the elbow and was repeatedly bent. The LM coil inside the sleeve maintained its electrical connection after 100 bends. Figure 8(d) shows photographs of the washing test. The cardigan was washed repeatedly using a washing machine. The impedance of the coil inside the cardigan increased by 1.7% after 100 washes. These results indicate that WPT clothes are highly durable against everyday mechanical deformation.

CONCLUSIONS

This study proposes an LM-based meandered coil with distributed capacitors using the friction jointing method for the full-body WPT clothing and demonstrates its stretch and bending tolerance. While the stretch tolerance was mainly affected by the frictional force, the bending tolerance was affected by the frictional force, the bending stiffness of the capsule, and the difference in the bending stiffness between the capsule and tube, and these factors were in a trade-off relationship. By optimizing the capsule shapes experimentally, the frictional jointing method achieved 3.1 times higher stretch tolerance and 3.5 times higher bending tolerance than the conventional adhesive jointing method. Furthermore, we fabricated the prototype of WPT clothing, cardigans, sleeves, and trousers, and demonstrated WPT and repeated stretching and washing. Our full-body WPT technology can be integrated into various textile products and contribute to the development of sustainable wearable computing in everyday life.

ACKNOWLEDGEMENTS

This work was partly supported by the JST ACT-X JPMJAX21K6, the JST ACT-X JPMJAX21K9, and JSPS KAKEN 22K21343.

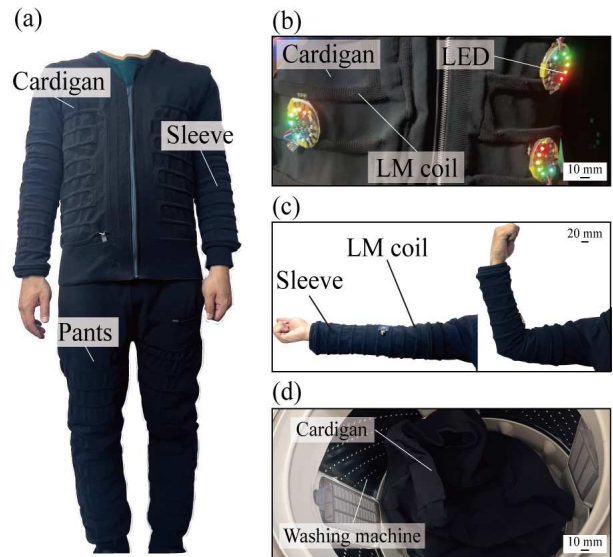


Figure 8 Photographs: (a) Prototype of the WPT clothing, (b) LED testing using WPT, (c) Bending tests, (d) Washing tests.

REFERENCES

- [1] X. Tian *et al.*, "Implant-to-implant wireless networking with metamaterial textiles," *Nat. Commun.*, vol. 14, no. 1, 4335, 2023.
- [2] R. Guo *et al.*, "Ni-GaIn amalgams enabled rapid and customizable fabrication of wearable and wireless healthcare electronics," *Adv. Eng. Mater.*, vol. 20, no. 10, 1800054, 2018.
- [3] R. Takahashi *et al.*, "Meander coil++: A body-scale wireless power transmission using safe-to-body and energy-efficient transmitter coil," *The Proceedings of the 2022 CHI Conference on Human Factors in Computing Systems*, art. no. 390, New Orleans LA USA, 2022.
- [4] R. Takahashi *et al.*, "Twin Meander Coil: Sensitive readout of battery-free on-body wireless sensors using body-scale meander coils," *Proc. ACM Interact. Mob. Wearable Ubiquitous Technol.*, vol. 5, issue 4, art. no. 179, 2021.
- [5] R. Takahashi *et al.*, "picoRing: battery-free rings for subtle thumb-to-index input," *The Proceedings of the 37th Annual ACM Symposium on User Interface Software and Technology*, art. no. 13, Pittsburgh PA USA, 2024.
- [6] T. Sato *et al.*, "High-accuracy contact resistance measurement method for liquid metal by considering current-density distribution in transfer length method measurement," *ACS Appl. Mater. Interfaces*, vol. 15, no. 37, pp. 44404–44412, 2023.
- [7] T. Sato *et al.*, "Method to reduce the contact resistivity between galinstan and a copper electrode for electrical connection in flexible devices," *ACS Appl. Mater. Interfaces*, vol. 13, no. 15, pp. 18247–18254, 2021.

CONTACT

T. Sato tel: +81-80-2185-3561

e-mail: machotakashi-satou@aist.go.jp